Journal of Applied Polymer Science

Photocatalytic properties of PMMA-TiO_2 class I and class II hybrid nanofibers obtained by electrospinning

Federico Ohlmaier-Delgadillo,[1] Maria Monica Castillo-Ortega,[1] Rafael Ramírez-Bon,[2] Lorena Armenta-Villegas,[1] Dora Evelia Rodríguez-Félix,[1] Hisila Santacruz- Ortega,[1] Teresa del Castillo-Castro,[1] Irela Santos-Sauceda[1]

[1]Departamento de Investigación en Polímeros y Materiales, Universidad de Sonora, Hermosillo, Sonora C.P. 83 000, Mexico
[2]Centro de Investigación y de Estudios Avanzados del IPN, Unidad Querétaro, Apdo, Postal 1-798, Querétaro, Qro, México
Correspondence to: M. M. Castillo-Ortega (E-mail: monicac@guaymas.uson.mx)

ABSTRACT: The preparation, characterization, and photocatalytic activity evaluation of three hybrid fibrous materials composed mainly by poly(methyl methacrylate) (PMMA), methyl methacrylate (MMA): 3-(trimethoxysilyl) propyl methacrylate (TMSPM): titanium butoxide (TBT), TiO_2 nanoparticles ($NPTiO_2$), and TiO_2 nanowires ($NWTiO_2$) is studied. Two types of fibers structures were prepared, single and core-shell structures. Scanning electron microscopy (SEM) and transmission electron microscopy (TEM) analysis showed both structures, single and core-shell, as well as the inorganic phase were dispersed in the hybrid fibers. Infrared spectroscopic analysis (FT-IR) and thermal analysis showed the organic and inorganic components, as well as the weight percentage of the inorganic phase present in hybrid fibers. The photocatalytic activity of the hybrid fibers class I and II showed that the best photodegradative efficiency for methylene blue in aqueous solution (2.9×10^{-5} M) was 95%, provided by PMMA—10 wt % $NPTiO_2$. © 2016 Wiley Periodicals, Inc. J. Appl. Polym. Sci. **2016**, *133*, 44334.

KEYWORDS: catalysts; electrospinning; fibers; nanoparticles; nanowires and nanocrystals

Received 18 February 2016; accepted 4 August 2016
DOI: 10.1002/app.44334

INTRODUCTION

Recently, the science community has been extremely interested in the study of organic–inorganic hybrid materials due to their ability to combine individual material characteristics with different chemical natures in a new material.[1,2] Nowadays, most of the studied hybrid materials are prepared using the sol-gel process, due to its many advantages such as its unique low-temperature processing, high purity, and well-controlled organic–inorganic composition through the incorporation of low molecular weight and oligomeric/polymeric molecules.[3] The actual availability of a great number of precursors for inorganic components through metal alkoxides (titanium butoxide), organo(alkoxi)silanes (3-(trimethoxysilyl) propyl methacrylate), and nanoparticles and their compatibility to the incorporation of polymerizable groups, such as methacryloxy, vinil, and epoxy groups, yield the possibility of obtaining a wide variety of hybrid sol-gel derived materials.[2]

Organic–inorganic hybrid materials have been classified according to chemical interactions presented between organic and inorganic parts in the new material. These interactions are responsible for the properties of the new resultant hybrid material. Class I hybrid material corresponds to hybrid systems where organic molecules, oligomers, or low molecular weight organic polymers are simply embedded in an inorganic matrix. Both components, organic and inorganic, exchange rather weak bonds, mainly through van der Waals force, hydrogen bonds, or ionic interactions. Class II corresponds to hybrid organic–inorganic composites, in which organic and inorganic components are bonded through stronger covalent or ionic-covalent chemical bonds.[2] Organic–inorganic hybrid materials have found technological applications in various areas, such as environmental and energy engineering.[4–7] In recent years, the demand for new materials in these areas has increased, and, in some cases, the design and production of these materials have been inspired specifically by nanometric scale fibers. Unlike other one-dimensional (1D) nanostructures such as nanowires and nanotubes, these nanofibers have a continuous structure, which provides them with high axial resistance and extreme flexibility. Consequently, nanofibers possess excellent mechanical properties.[8,9] Among the different existing methods for nanofiber preparation, the electrospinning technique has emerged as a versatile, effective, and inexpensive technique for continuous fiber production with diameters ranging from several micrometers to a few nanometers.[8,10,11]

Filtration systems offer a potential solution for a wide range of environmental issues, mainly for the treatment of sewage and air purification. The future of these systems is dependent on the preparation and production of new materials serving as an effective technology for environmental applications. Fibrous polymeric membranes obtained using the electrospinning technique represent an option that offers contaminant removal from the environment with low power consumption and low cost.[12–15] Yet, most of the recent studies related with filtration systems are favoring the use of only inorganic nanofibers for air and water purification, mainly because of their high photodegradation yield. However, inorganic nanofibers lack good mechanical properties due to the fact that the organic phase provides flexibility and handling properties to filtration systems.[16–19] As a result, hybrid nanofibers will combine both the photocatalytic activity from their inorganic nature and excellent mechanical properties from their organic nature.

PMMA is a linear thermoplastic polymer, which possesses great mechanical resistance, high Young's modulus, and low elongation at break. Also, PMMA presents low capacity to absorb water. As a result, PMMA derivative products have excellent dimensional stability and can be used in filtration systems.[20,21]

TiO_2 is the photocatalyst mostly used for water and air purification not only because its obtaining process is relatively inexpensive, but also because it is an abundant material in nature. Rutile, anatase, and brookite, are three known crystalline structures of TiO_2. Of these three crystalline structures, anatase is the one mainly used as a photocatalyst under UV irradiation.[21,22]

Hybrid fibrous polymeric membranes of PMMA and TiO_2 represent an option for the treatment of aqueous systems because the combination of both compounds provides unique qualities to the fibrous membrane generated by the electrospinning technique, such as excellent mechanical properties brought from PMMA and photocatalytic properties from TiO_2.

Preparation, characterization, and the photocatalytic activity of three new hybrid materials is studied, focusing on the environmental area. Using the electrospinning technique, core-shell hybrid fibers were prepared from PMMA and a hybrid sol-gel solution of MMA: TMSPM: TBT, and single fibers were prepared from PMMA, TiO_2 nanoparticles, or TiO_2 nanowires. In addition, comparative photodegradation activity studies were performed to class I and class II hybrid materials in order to determine their methylene blue photodegradation efficiency.

EXPERIMENTAL

Materials

Hybrid fibers titania-poly(methylmethacrylate) class I were prepared using commercial grade acetone obtained from Faga Lab. Poly(methyl methacrylate) (PMMA) (molecular weight of 350,000 g/mol), titanium dioxide nanoparticles ($NPTiO_2$) (<25 nm, anatase), and titanium dioxide nanowires ($NWTiO_2$) (diameter ~100 nm, length ~10 μm) were obtained from Sigma-Aldrich. Hybrid fibers titania–poly(methylmethacrylate) class II were prepared using titanium butoxide (TBT) as the inorganic precursor,[17,23] methyl methacrylate (MMA) (molecular weight of 100.12 g/mol) as the source of organic component, 3-(trimethoxysilyl) propyl methacrylate (TMSPM) as the coupling agent,[1,3] and ethanol (EtOH) as the solvent. Distilled and deionized water and benzoyl peroxide (BPO) used as the initiators for polymerization, were obtained from Sigma-Aldrich.

Preparation of Hybrid Fibers Class I and Class II

The class I and class II hybrid fibers with various amounts of titania were prepared controlling three main parameters of the electrospinning technique: voltage, distance between stainless steel capillary and aluminum collector, and flow of the polymeric solution. First, a 6 wt % solution of PMMA and acetone was prepared by dissolving 3 g of PMMA in 50 mL of acetone. The solution was continually maintained in magnetic stirring for 24 h at room temperature. Second, a precursor class I hybrid solution of $NPTiO_2$ and $NWTiO_2$ was prepared at diverse concentrations, 1, 5, 10, and 15 wt %, respectively. Third, a class II hybrid precursor solution of MMA: TMSPM: TBT was prepared at a 1:1:1 molar ratio by mixing the adequate amount of reagents. Then the class II hybrid precursor solution (MMA: TMSPM: TBT) was mixed with the PMMA solution in order to obtain two class II hybrid solutions. As a result, two precursor class II hybrid solutions of 2:1 and 4:1 volume/volume (V/V) ratios were prepared. Once the precursor hybrid solutions were ready, 5 mL of class I hybrid solution (PMMA + $NPTiO_2$ and PMMA + $NWTiO_2$) was transferred to a 6 mL plastic syringe and then placed in the electrospinning equipment. The hybrid fibers class II were electrospun by coaxial arrangement. A 6 mL plastic syringe within a nozzle of 13.9 mm inner diameter (i.d) was filled with 5 mL of PMMA solution. A 6 mL plastic syringe within a nozzle of 8 mm i.d was filled with 6 mL of class II hybrid solution. Both syringes, the one containing PMMA solution and the other one containing class II hybrid solution, were joined together by the nozzle tip with the smaller diameter inside the larger diameter. The hybrid solutions were supplied by a syringe pump (Kd Scientific) and the feed rate varied from 4.0 to 0.2 mL h^{-1} at 0.1 mL h^{-1} intervals. The metallic needle was connected to a high-voltage power supply (Spellman CZE 1000R). The voltage was increased from 14 to 20 kV. The hybrid fibers were collected on an aluminum foil sheet (10 cm × 10 cm). The distance between the nozzle tip and the collector was varied from 15 to 45 cm.

Scanning Electron Microscopy

Surface characterization and the average diameter of the hybrid fibers were performed using a scanning electron microscope (SEM) JEOL5410LV equipped with a INCA dispersive X-ray detector system (Oxford Instrument) and operated at a voltage of 20 kV. Samples were coated with gold before being observed under a high vacuum using the secondary electron detector. The average diameter of the fibers was determined from the SEM images of the fibers (1500× magnification) using ImageJ software. At least 30 different fibers were measured for each experimental condition.

Transmission Electron Microscopy

The morphological characterization and the distribution of $NPTiO_2$ and $NWTiO_2$ inside the hybrid fibers were performed using a transmission electron microscope JEOL jem-2010f.

Samples without any pretreatment were placed between two copper mesh grids that had 50 to 400 holes per inch.

Infrared Spectroscopic Analysis

Fourier transform-infrared spectroscopy (FT-IR) analysis was performed with a Perkin-Elmer Spectrum GX FT-IR spectrometer. A Spectrum scan was performed from 4000 cm^{-1} to 400 cm^{-1} Approximately 1 mg of the sample was mixed with KBr directly to form a pellet, the mixing ratio (KBr: sample) was 60:1 and the measurements were performed in transmittance mode.

Thermal Analysis

The thermal behavior of the materials was studied by thermogravimetric analysis (TGA) using a Perkin-Elmer model Pyris 1 TGA instrument. About 2 mg of the sample were placed in the sample holder of alumina and was subjected to a temperature increase at a rate of 10 °C min^{-1} from 25 °C to 600 °C in a nitrogen flow, and from 600 °C to 800 °C in an oxygen flow.

Analysis of Micromechanical Properties

The micromechanical properties of the hybrid fibers were measured in tension mode, using a Honeywell load cell, an intelligent picomotor, New Focus model 8753, connected to a New Focus picomotor actuator, in order to obtain the values of tensile strength, maximum elongation, and Young's modulus. Specimens were cut in a dog bone shape (38 mm × 15 mm overall in size, 5 mm × 22 mm in the gauge area) as indicated in ASTM D1708. At least seven specimens of each film were tested as indicated and the average values are reported. The thickness of the films was measured with a Mitutoyo micrometer. The tests were performed using a load cell with a range from zero to 150 g with a maximum speed of 1.2 mm/min.

Photocatalytic Activity of Hybrid Fibers Class I and Class II Composed by PMMA and TiO_2

The photocatalytic activity of the hybrid fibers class I and II was analyzed by photodegradation of methylene blue (MB, Sigma- Aldrich) 2.9×10^{-5} M in aqueous solution directly from the reaction system. This reaction system consisted of a plastic UV-Vis cuvette (width: 1 cm, length: 1 cm, height: 5 cm, Kartell) filled with 3 mL of MB solution and 2 mg of each hybrid fibers. The photodegradation UV-Vis absorption spectra of methylene blue was obtained by Agilent 8453 UV-Visible Spectroscopy System. The Ultraviolet light was provided by an UV source (355–360 nm) Ushio F6T5BL 3000110, 6 W. The cuvette was placed at a distance of 10 cm from the UV source. Before UV irradiation, the reaction system was subjected to ultrasonic agitation in the absence of light for 10 min in order to establish the conditions of adsorption–desorption equilibrium. For analytical purposes there was no water flow during the photodegradation process. At regular time intervals of 4 h, the dye concentration was measured by using UV-Vis spectrophotometer. The remaining concentration of MB after reaching adsorption–desorption equilibrium (C_0) and during photodegradation process (C) was determined by UV-Vis spectroscopy by observing the band changing at 660 nm. Photodegradation efficiency is expressed graphically with the relation C/C_0. The experiment was performed threefold for each of the hybrid fibrous.

RESULTS AND DISCUSSION

Optimal Conditions for Preparation of Hybrid Fibers Class I and Class II

In order to get fibers with continual and no agglomerate shape, the effect of varying the electrospinning conditions on the fiber's morphology was studied. After a systematic study, varying the conditions for both single and the coaxial electrospinning methods, the optimal conditions for the preparation class I and class II PMMA hybrid fibers were found, using various amounts of titania. The optimal flow rate for the PMMA fibers was 4 mL h^{-1}. The applied voltage was 18 kV and the distance between the nozzle tip and the collector was 15 cm. The optimal conditions for preparing hybrid fibers class I varied while the amount of $NPTiO_2$ and $NWTiO_2$ increased. The flow rate for the hybrid solution class I composed by PMMA—1 wt % $NPTiO_2$ and PMMA—1 wt % $NWTiO_2$ was 4 mL h^{-1}, the applied voltage was 18 kV, and the distance between the nozzle tip and the collector was 16 cm. Both hybrid fibers were composed by 5 and 10 wt % ($NPTiO_2$ or $NWTiO_2$), the applied voltage was 18 kV, the flow rates were 3.5 or 3 mL h^{-1}, and the distances between the nozzle tip and the collector were 16 and 30 cm, respectively. The PMMA—15wt % $NPTiO_2$ and PMMA—15wt % $NWTiO_2$ hybrid fibers were prepared by 3 mL h^{-1} of the flow rate, a voltage of 18 kV, and 45 cm of distance between the nozzle tip and the collector. The optimal conditions for preparation of hybrid fibers class I composed by various amounts of $NPTiO_2$ and $NWTiO_2$ were the same in each concentration due to the fact that the only variant was the morphology of the inorganic phase as presented in Figure 1. For both hybrid fibers class II (2:1 V/V and 4:1 V/V), the optimal flow rates were 1.5 and 2.2 mL h^{-1}. The applied voltage was 20 kV and the distance between the nozzle tip and the collector was 20 cm. Table I summarizes the optimal conditions for the preparation of hybrid fibers class I and II.

Morphological and Spectroscopic Properties

Morphology: SEM and TEM. Both SEM and TEM enabled the study of the hybrid fiber morphology and the distribution of the inorganic phase on the hybrid fibers. Figure 1 shows the SEM micrographs for the PMMA fibers and hybrid fibers class I and class II at a 1500× magnification. PMMA fibers with a smooth, nonporous, and cylindrical shape are shown in Figure 1(a). The average diameter of PMMA fibers was 1.35 ± 0.44 μm. In Figure 1(b,c), PMMA hybrid fibers class I with 1 and 15 wt % $NPTiO_2$ are shown. Figure 1(b) represents the SEM micrographs of hybrid fibers with 1 wt % $NPTiO_2$. As shown in Figure 1(b), the hybrid fibers are uniform and smooth in appearance (it should be noted that the morphology of the hybrid fibers with 1 wt % $NPTiO_2$ lack agglomerate or beads, acquiring a cylindrical, nonporous structure with an average diameter of 1.55 ± 0.39 μm). Hybrid fibers with 15 wt % $NPTiO_2$ and an average diameter of 1.7 ± 1.29 μm are represented in Figure 1(c), it can be observed that at this concentration of the inorganic phase, the presence of agglomerations or beads in the morphology of the fibers is very notable. The presence of these clumps can be attributed to poor $NPTiO_2$ dispersion at the time of forming fibers in the electrospinning technique. It is important to emphasize that hybrid fibers with

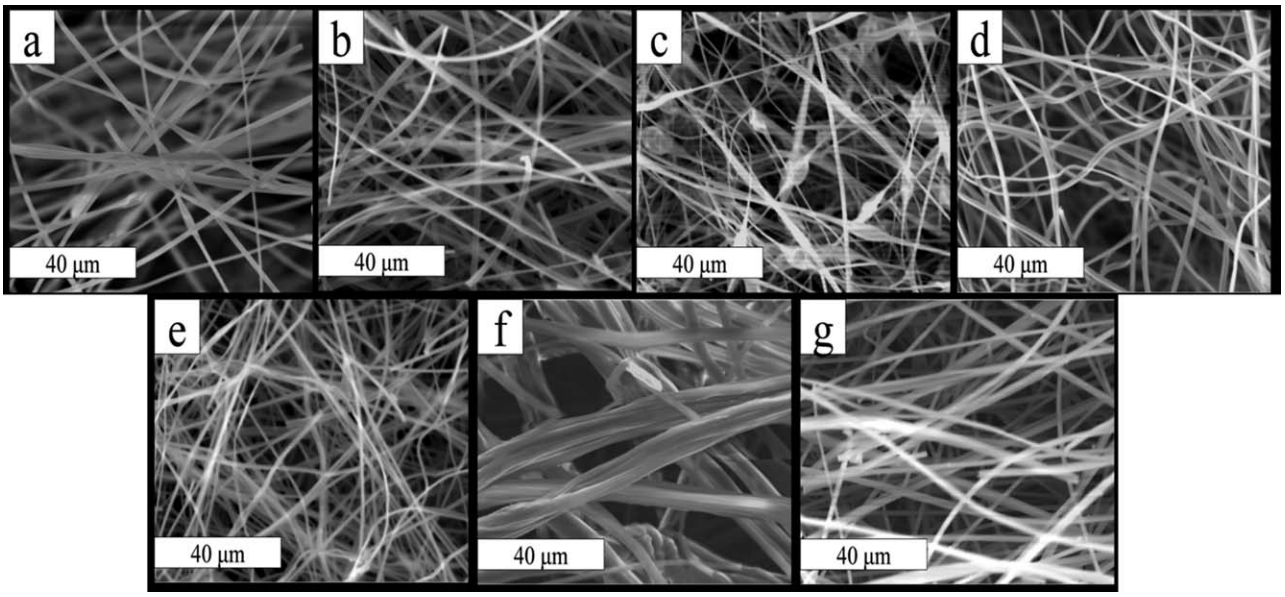

Figure 1. SEM micrographs of fibers (a) PMMA, hybrid fibers class I (b) 1 wt % $NPTiO_2$ (c) 15 wt % $NPTiO_2$ (d) 1 wt % $NWTiO_2$ (e) 15 wt % $NWTiO_2$, hybrid fibers class II (f) PMMA/MMA: TMSPM: TBT [2:1] (g) PMMA/MMA: TMSPM: TBT [4:1], at 1500× magnification.

5 wt % $NPTiO_2$ and 10 wt % $NPTiO_2$ were similar in morphology to PMMA—1 wt % $NPTiO_2$ hybrid fibers. Moreover, PMMA—1 wt % $NWTiO_2$ hybrid fibers [Figure 1(d)] had an average morphology and diameter (1.51 ± 0.5 μm) similar to PMMA—1 wt % $NPTiO_2$ hybrid fibers due to the same concentration of inorganic phase. Apparently, the structure difference between the nanowires and nanoparticles does not affect the morphology of the hybrid fibers at low concentrations. Figure 1(e) shows the micrograph of PMMA—15 wt % $NWTiO_2$ hybrid fibers with an average diameter of 1.18 ± 0.36 μm without any apparent defect, unlike PMMA—15 wt % $NPTiO_2$ hybrid fibers where the presence of agglomerations and beads in the morphology of the fibers were very notable. On the other hand, PMMA—5 wt % $NWTiO_2$ hybrid fibers and PMMA—10 wt % $NWTiO_2$ hybrid fibers followed the same morphological behavior of PMMA—1 wt % $NWTiO_2$ hybrid fibers. Figure 1(f) shows the micrograph of PMMA/MMA: TMSPM: TBT [2:1] hybrid fibers. It is observed that the morphology of the resulting hybrid fibers from the 2:1 V/V ratio solution in coaxial arrangement promotes the formation of fibers heaped together as well as the increase in the average diameter of fibers from 1.35 μm (PMMA) to 4.7 ± 1.99 μm. Finally, Figure 1(g) shows the micrograph of PMMA/MMA: TMSPM: TBT [4:1] hybrid fibers and clearly illustrates that at a 4:1 V/V ratio, soft and uniform hybrid fibers are formed. In addition, 4:1 V/V ratio hybrid fibers showed an average diameter slightly above pure PMMA fibers, of 1.48 ± 0.34 μm. This result is attributed to the proper formation of the shell, which is constituted only within the hybrid solution.

Table I. Optimal Conditions for the Preparation of Hybrid Fibers Class I and Class II

Fibers	Voltage (kV)	Feed rate (mL h^{-1})	Distance (cm)
PMMA	18	4	15
PMMA—1 wt % $NPTiO_2$	18	4	16
PMMA—5 wt % $NPTiO_2$	18	3.5	16
PMMA—10 wt % $NPTiO_2$	18	3	30
PMMA—15 wt % $NPTiO_2$	20	3	45
PMMA—1 wt % $NWTiO_2$	18	4	16
PMMA—5 wt % $NWTiO_2$	18	3.5	16
PMMA—10 wt % $NWTiO_2$	18	3	30
PMMA—15 wt % $NWTiO_2$	20	3	45
PMMA/MMA: TMSPM: TBT 2:1 V/V	20	1.5	20
PMMA/MMA: TMSPM: TBT 4:1 V/V	20	2.2	20

Figure 2 shows the TEM micrographs for the PMMA fibers and hybrid fibers class I and class II at a 4000× magnification. Figure 2(a) confirms the soft (nonporous) morphology of PMMA fibers. Figure 2(b) shows the presence of $NPTiO_2$ on PMMA—1 wt % $NPTiO_2$ hybrid fiber. Figure 2(c) shows PMMA—15 wt % $NPTiO_2$ hybrid fiber in which the presence of $NPTiO_2$ is observed. Also, it can be demonstrated that the presence of beads on the hybrid fibers observed in Figure 1(c) is an effect caused by the agglomeration of $NPTiO_2$ on PMMA fibers at the time of its preparation, which leads to the hypothesis that there is an effect of $NPTiO_2$ saturation on PMMA fibers. Figure 2(d,e) illustrate the TEM micrographs for both hybrid fibers, 1 wt % $NWTiO_2$ and 15 wt % $NWTiO_2$, in which the presence of $NWTiO_2$ is observed. It is visible that at a concentration of 15 wt % $NWTiO_2$, the hybrid fibers had no beads in its morphology—as shown in Figure 2(e). This occurrence is explained not only due to the fact that the $NWTiO_2$ did not saturate the fibers, but also because the $NWTiO_2$'s elongated structure provided stability

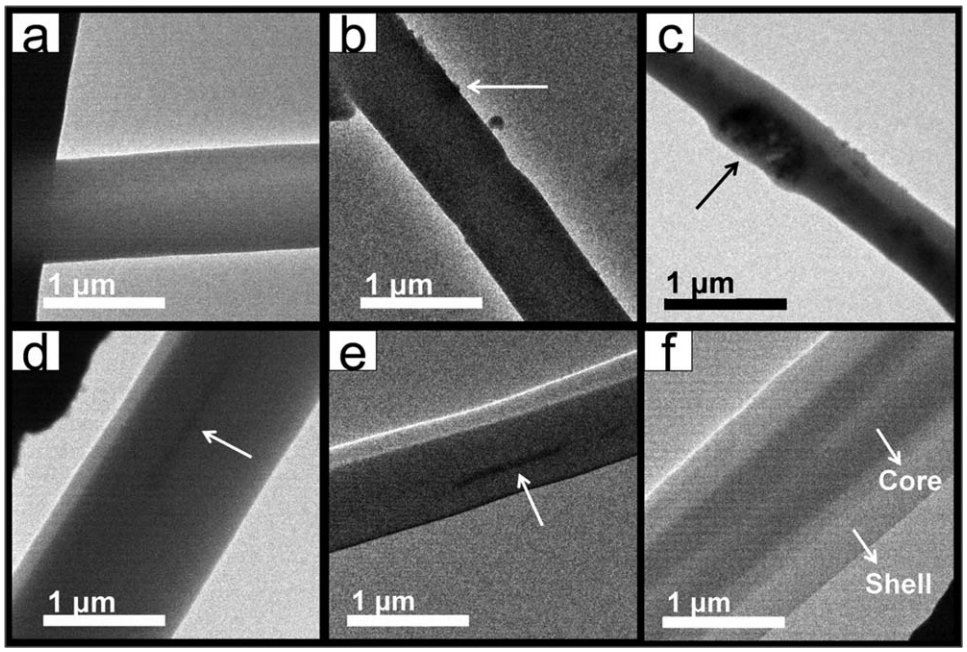

Figure 2. TEM micrographs of fibers (a) PMMA, hybrid fibers class I (b) 1 wt % $NPTiO_2$, (c) 15 wt % $NPTiO_2$, (d) 1 wt % $NWTiO_2$, (e) 15 wt % $NWTiO_2$, hybrid fibers class II, (f) PMMA/MMA: TMSPM: TBT [4:1].

to the acquired morphology with fibers allowing a better interaction between titanium dioxide ($NWTiO_2$) and acrylate group (organic phase), which is more attainable in wire-like forms than globe-like forms ($NPTiO_2$). Figure 2(f) shows the micrograph of PMMA/MMA: TMSPM: TBT [4:1] hybrid fiber. The acquired core-shell structure where the core is compounded by PMMA and the class II PMMA-TiO_2 hybrid material shell is noticeable.

SEM and TEM micrographs demonstrated that the morphology acquired by hybrid fibers is presented in terms of the inorganic amount and the conditions of the electrospinning technique. Additionally, it was observed that wire shape from $NWTiO_2$ promoted the formation of continual fibers without agglomerations. In contrast, particle shape from $NPTiO_2$ promoted the formation of fibers with agglomerations at the highest concentrations. Otherwise, we found that as the amount of TiO_2 increased at the precursor solution during the electrospinning technique, the amount of fibers formed on the aluminum collector declined, as a result of a decrease in handleability of hybrid fibers.

FT-IR Characterization. FT-IR spectra are shown in Figure 3. Figure 3(a) shows the characteristic peaks of PMMA, the peaks representing C—H stretching 2997 cm^{-1} and 2950 cm^{-1} and C═O stretch at 1735 $cm^{-1}$and C-H stretch at 1448 cm^{-1} Figure 3(b) shows the characteristic peak of $NPTiO_2$ with a Ti-O stretch in a wave number ranging from 500 to 790 cm^{-1}.[24] Figure 3(c,d) show the characteristics peaks of both organic and inorganic phases in PMMA—1 wt % $NPTiO_2$ and PMMA—15 wt % $NPTiO_2$ hybrid fibers class I. The main peaks are the C═O stretch at 1735 cm^{-1} and the Ti-O stretch in a wave number ranging from 500 to 790 cm^{-1}. Figure 3(e) shows the characteristic peak of $NWTiO_2$ with a Ti-O stretch at 505 cm^{-1}.[24] Figure 3(f,g) shows the characteristics peaks of both organic and inorganic phases in PMMA—1 wt % $NWTiO_2$ and PMMA—15 wt % $NWTiO_2$ hybrid fibers class I. At higher $NWTiO_2$ concentration, the peak at 505 cm^{-1} is wider. Figure 3(h,i) show the characteristic peaks of both organic and inorganic phases in PMMA/MMA: TMSPM: TBT 2:1 V/V and PMMA/MMA: TMSPM: TBT 4:1 V/V hybrid fibers class II. The PMMA characteristic peak at 1735 cm^{-1} is presented in both Figure 3(h,i). The inorganic phase presence is demonstrated by the appearance of a new peak at 1630 cm^{-1} as demonstrated by Du *et al.*,[25] who observed that the intensity of this band increased with an increasing TiO_2 content in the prepared films, this band does not appear in the spectrum of PMMA. Chen *et al.*[26] assigned the same signal to the possible interaction between the acrylate group and TiO_2. On the other hand, the peaks at 3650 cm^{-1} and 3420 cm^{-1} are characteristic of O-H stretch, which are typical of the present species in the hybrid precursor solution. It can be noticed from Figure 3(h,i) that the new formed peak at 1630 cm^{-1} decreased in intensity in the 4:1 V/V ratio because the amount of hybrid solution is lower than at a 2:1 V/V ratio. Table II shows FT-IR information of functional groups present in the materials.

Thermal Analysis

Figure 4 shows the weight loss and heat flow for PMMA fibers, hybrid fibers class I, and hybrid fibers class II. The degradation of PMMA fibers is observed in one step, the final degradation temperature was 360.2 °C. The thermograms of hybrid fibers class I confirmed the exact amount of inorganic phase present in them, as shown in Figure 4(a,b). As seen in Figure 4, all these thermograms show degradation in one step; however, the final degradation temperature was slightly different for each hybrid fiber class I [Figure 4(a,b)], depending on the inorganic phase concentration. In the case of PMMA—1 wt % $NPTiO_2$ and PMMA—1 wt % $NWTiO_2$ hybrid fibers, the residual

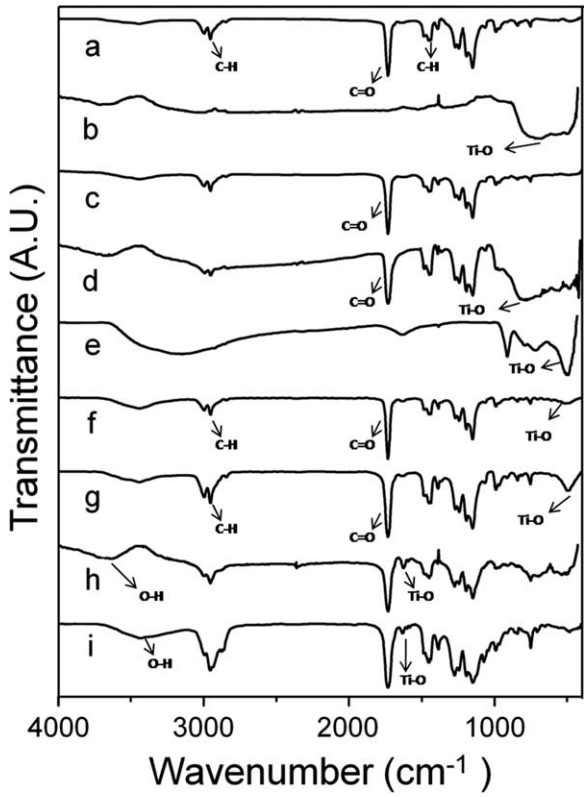

Figure 3. FT-IR of (a) PMMA, (b) $NPTiO_2$, (c) PMMA—1 wt % $NPTiO_2$, (d) PMMA—15 wt % $NPTiO_2$, (e) $NWTiO_2$, (f) PMMA—1 wt % $NWTiO_2$, (g) PMMA—15 wt % $NWTiO_2$, (h) PMMA/MMA: TMSPM: TBT 2:1 V/V, (i) PMMA/MMA: TMSPM: TBT 4:1 V/V.

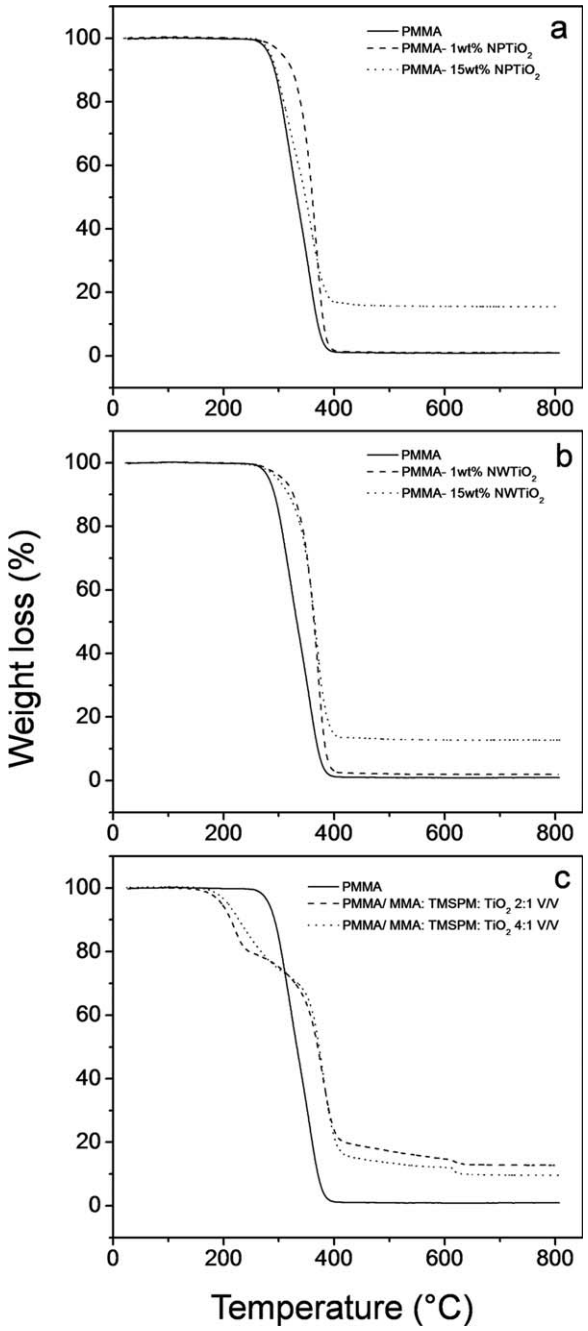

Figure 4. TGA curves for PMMA fibers, hybrid fibers class I (a) PMMA + $NPTiO_2$, (b) PMMA + $NWTiO_2$ and (c) PMMA/MMA: TMSPM: TBT hybrid fibers class II.

weights were 1.1% and 1.8% of the original fibers weight, as shown in Figure 4(a,b). These residual weights corresponded to the inorganic phase. On the other hand, the final degradation temperatures for those fibers were 370.2 °C and 372.3 °C, 12 °C, higher than PMMA fibers in the case of PMMA—1 wt % $NWTiO_2$ hybrid fibers. The PMMA—15 wt % $NPTiO_2$ and PMMA—15 wt % $NWTiO_2$ hybrid fibers had 15.7% and 13.7% of residual weight. Also, Figure 4(a,b) show that the degradation temperatures for those hybrid fibers were 364.46 °C and 370.4 °C. After the addition of $NPTiO_2$ and $NWTiO_2$, the thermal stability of the PMMA fibers increases noticeably. Friederich *et al.*[27] described this behavior only in PMMA + $NPTiO_2$ systems, due to the possible restriction on the mobility of PMMA chains, caused by the presence of nanoparticles and/or a reaction between the polymer and the nanoparticles surface through the methoxycarbonyl group. Both PMMA/MMA: TMSPM: TBT 2:1 V/V and PMMA/MMA: TMSPM: TBT 4:1 V/V hybrid fibers class II presented two steps of degradation [shown in Figure 4(c)]. In the case of PMMA/MMA: TMSPM: TBT 2:1 V/V, the first step at 225.9 °C corresponds to the degradation of the hybrid precursor solution, and the second degradation step being at 378.8 °C, a close temperature to the PMMA degradation temperature. Nevertheless, the second degradation step is presented at a higher temperature than PMMA thermal

Table II. FT-IR Functional Groups

Wave length (cm^{-1})	Functional group	Component
3650-3420	Alcohol	O—H
2997	Alkane	C—H
2950	Alkane	C—H
1735	Ester	C=O
1630	Inorganic	Ti—O
1448	Alkane	C—H
500-790	Inorganic	Ti—O

Table III. Micromechanical Properties of PMMA Fibers, Hybrid Fibers Class I, and Hybrid Fibers Class II

Fibers	Tensile strength (MPa)	Young's modulus (MPa)	Elongation at break (%)
PMMA	0.028 ± 0.007	0.54 ± 0.23	10.31 ± 2.19
PMMA—1 wt % $NPTiO_2$	0.081 ± 0.002	0.54 ± 0.41	7.28 ± 1
PMMA—5 wt % $NPTiO_2$	0.017 ± 0.005	0.22 ± 0.05	14.74 ± 3.04
PMMA—10 wt % $NPTiO_2$	0.035 ± 0.008	0.91 ± 0.55	13.98 ± 2.33
PMMA—15 wt % $NPTiO_2$	0.007 ± 0.007	0.19 ± 0.11	9.3 ± 3.75
PMMA—1 wt % $NWTiO_2$	0.306 ± 0.11	3.84 ± 0.93	17.12 ± 3.48
PMMA—5 wt % $NWTiO_2$	0.13 ± 0.009	2.62 ± 0.71	16.33 ± 0.77
PMMA—10 wt % $NWTiO_2$	0.089 ± 0.024	2.1 ± 0.66	19.8 ± 4
PMMA—15 wt % $NWTiO_2$	0.06 ± 0.02	1.6 ± 0.64	15.41 ± 1.62
PMMA/MMA: TMSPM: TBT 2:1 V/V	0.03 ± 0.004	1.91 ± 0.98	9.18 ± 1.86
PMMA/MMA: TMSPM: TBT 4:1 V/V	0.44 ± 0.13	36.37 ± 7.71	3.73 ± 0.64

degradation, a behavior observed by Du *et al.*,[25] who attributed it to the possible interaction between the PMMA matrix and the inorganic phase. Finally, the first weight loss for PMMA/MMA: TMSPM: TBT 4:1 V/V hybrid fibers is at 231.1 °C, a slightly higher temperature than the first degradation step of PMMA/MMA: TMSPM: TBT 2:1 V/V hybrid fibers. It is noteworthy that this result coincides with the fact that there is a larger proportion of PMMA than hybrid material on fibers, so the first degradation step moved to a closer PMMA degradation temperature. Even with the PMMA-rich composition of these fibers, the slight increase of the PMMA degradation temperature evidences the stronger interaction of the organic and inorganic phases. In fact, it can be observed that the thermograms of these fibers continue decreasing at temperatures higher than 400 °C and up to 600 °C. This weight loss can be attributed to polymer chains that require higher energy to break because they have an even stronger interaction with the inorganic phase, which encloses them and limits their movement as expected in these hybrid fibers class II. Also, the last weight loss observed at 600 °C is due to the gas flow changed from nitrogen to oxygen where the remaining organic compounds were degraded.

Analysis of Micromechanical Properties

Table III shows the tensile strength, Young's modulus, and the elongation at break of PMMA fibers of hybrid fibers class I and hybrid fibers class II. In the case of hybrid fibers class, I, all the hybrid fibers composed by PMMA + $NWTiO_2$ had better micromechanical properties than hybrid fibers composed by PMMA + $NPTiO_2$. PMMA—1 wt % $NWTiO_2$, hybrid fibers exhibited the highest tensile strength, suggesting that 1 wt % $NWTiO_2$ increases the ability of fibers to withstand a greater amount of applied strength before its permanent deformation. In both cases, hybrid fibers composed by PMMA + $NPTiO_2$ and PMMA + $NWTiO_2$ result in a reinforced effect of PMMA fibers at small concentrations of $NPTiO_2$ and $NWTiO_2$. This effect can be attributed to a good dispersion of inorganic phase at small concentrations. In the same way, the fibers with 1wt % $NWTiO_2$ presented the highest Young's modulus value, which means that at this concentration the rigidity of the material has increased. In addition, it can be inferred that at a low inorganic phase concentration, the interaction between titanium dioxide ($NWTiO_2$) and acrylate group increases the Young's modulus, providing more flexibility to the fibers. In the case of hybrid fibers class II, PMMA/MMA: TMSPM: TBT 4:1 V/V hybrid fibers not only exhibited the highest tensile strength indicating a greater interaction effect among acrylate group and TiO_2, but also it shows the highest Young's modulus value. Although, PMMA/MMA: TMSPM: TBT 2:1 V/V hybrid fibers showed larger diameter than 4:1 V/V hybrid fibers, fibers are agglomerated [Figure 1(f)], and this characteristic is affecting directly their mechanical properties. It is important to note that the fiber's morphology significantly influences the mechanical properties as noticed in hybrid fibers class II, where the Young's modulus value increased 20 times for 4:1 V/V fibers, compared to 2:1 V/V fibers. Even though PMMA fibers and most of the hybrid fibers except PMMA/MMA:TMSPM:TBT 4:1 V/V showed low mechanical properties, these fibers are handleable enough to be processed during the photocatalytic test, mainly because the photocatalytic activity was measured with no water flow as mentioned in Photocatalytic Activity of Hybrid Fibers Class I and Class II Composed by PMMA and TiO_2 section.

Photocatalytic Activity of Hybrid Fibers Class I and Class II Composed by PMMA and TiO_2

Figure 5 shows the photodegradation efficiency of methylene blue for PMMA fibers, hybrid fibers class I, and hybrid fibers class II. As shown in Figure 5, the control sample of PMMA fibers had approximately 15% of photodegradation efficiency due to the UV irradiation effect onto MB molecules. The interaction between MB molecules and UV irradiation affected the organic molecule stability; as a result, MB molecules were removed. Figure 5(a) corresponds to the graphics of efficiency for hybrid fibers composed by PMMA + $NPTiO_2$. Photodegradation efficiency obtained by PMMA—1 wt % $NPTiO_2$ fibers after 28 h was approximately 85%. The efficiency obtained by PMMA—5 wt % $NPTiO_2$ fibers was 91%. The efficiency of 94% and 93% were for PMMA—10 wt % $NPTiO_2$ fibers and PMMA—15 wt % $NPTiO_2$ fibers, respectively. It can be concluded that as the concentration of $NPTiO_2$ was increasing in the fibers, the photodegradation efficiency also increased. However, in hybrid fibers with the highest $NPTiO_2$ concentration, the efficiency was not the greatest, mainly because the presence

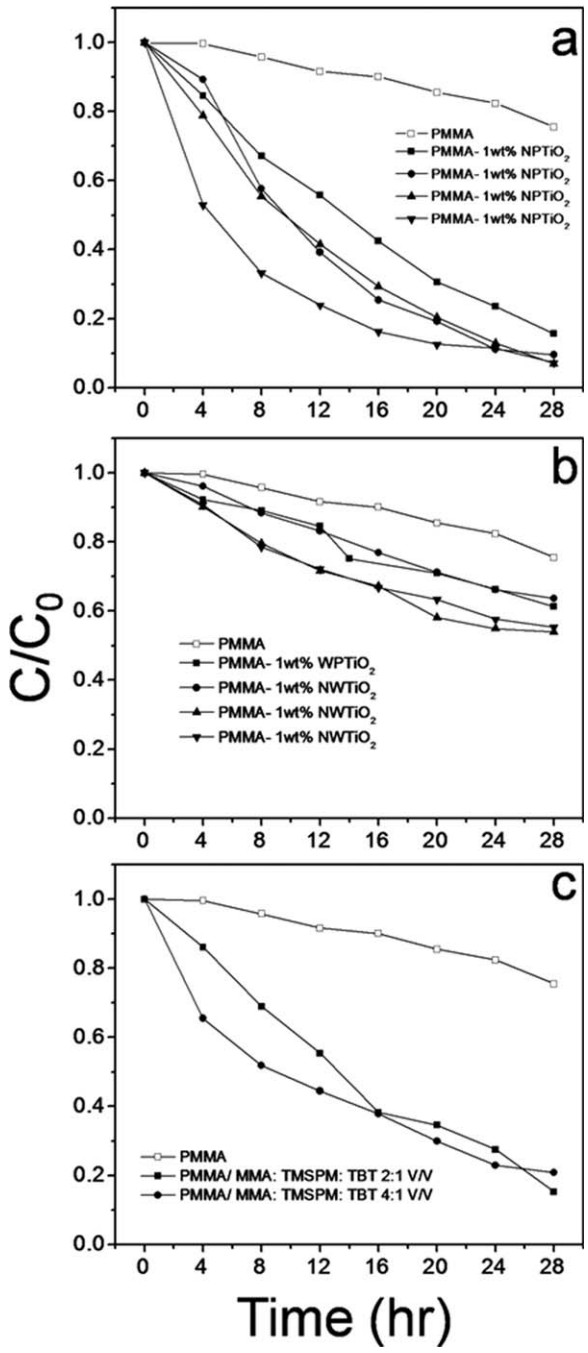

Figure 5. Photodegradation efficiency of methylene blue (C/C_0 determined by the band changing at 660 nm) for hybrid fibers class I (a) PMMA + $NPTiO_2$, (b) PMMA + $NWTiO_2$, and (c) PMMA/MMA: TMSPM: TBT hybrid fibers class II.

of $NPTiO_2$ agglomerates affected the photodegradation process by decreasing the production of hydroxyl radicals (OH-) generated during the $NPTiO_2$ activation process with ultraviolet light. These radicals worked to breakdown the MB molecules. Furthermore, the inadequate distribution of $NPTiO_2$ observed on PMMA—15 wt % $NPTiO_2$ hybrid fibers can affect the production of hydroxyl radicals during the photodegradation process. This could be due to the presence of $NPTiO_2$ agglomerates observed on the fibers. Figure 5(b) corresponds to the graphics of efficiency for hybrid fibers composed by PMMA + $NWTiO_2$. Photodegradation efficiency obtained by PMMA—1 wt % $NWTiO_2$ fibers at the end of 28 h was approximately 39%. The efficiency obtained by PMMA—5 wt % $NWTiO_2$ fibers was 37%. The efficiency of 47% and 45% were for PMMA—10 wt % $NWTiO_2$ fibers and PMMA—15 wt % $NWTiO_2$ fibers. It is possible that hybrid fibers composed by PMMA + $NWTiO_2$ showed lower photodegradation efficiency than hybrid fibers composed by PMMA + $NPTiO_2$ because anatase might be less in proportion compared to rutile and brookite. Figure 5(c) corresponds to the graphics of photodegradation efficiency for hybrid fibers class II. The photodegradation efficiency of hybrid fibers with 2:1 V/V ratio was approximately 85% and 80% for hybrid fibers with a 4:1 V/V ratio. The 5% difference is due to the amount of precursor hybrid solution presented on fibers, since it is where TiO_2 and SiO_2 (from TMSPM) are found. Apparently, the morphology acquired by hybrid fibers class II did not negatively affect the photodegradation efficiency, since the fibers with 2:1 V/V ratio presented greater efficiency as well as a tendency to form clumps among fibers. It is important to note that the photodegradation efficiency of these hybrid fibers is not so different from that of the class I hybrid fibers, with similar inorganic content (15% $NPTiO_2$), despite the amorphous characteristic of the inorganic phase in the class II hybrid fibers. Furthermore, class II hybrid fibers were processed at room temperature; whereas commercial $NPTiO_2$ in class I hybrid fibers required much higher processing temperature to reach the anatase crystalline phase. Therefore, the low processing temperature of class II hybrid fibers indeed represents an important advantage as photocatalyst materials. Even though these new hybrid materials reached a 94% photodegradation yield after 28 h in process, they have an excellent potential usage for filtration systems in aqueous environments because of their mechanical properties and low cost of production process, especially class II hybrid fibers.

CONCLUSIONS

Optimal conditions for the preparation of three hybrid materials based on PMMA and TiO_2 were found using the electrospinning technique. Two new types of fibrous hybrid materials class II with core-shell structure were prepared, PMMA/MMA: TMSPM: TBT 2:1 V/V and PMMA/MMA: TMSPM: TBT 4:1 V/V. Both materials presented differences between diameters and morphology, primarily governed by the concentration of hybrid solutions in fibers. Also, SEM and TEM determined the morphological characteristics brought from a simple, mixed solution process and a sol-gel technique for hybrid fibers class I and hybrid fibers class II. In addition, these two techniques demonstrated that the acquired morphology by hybrid fibers class I depended not only on the inorganic phase concentration, but also on the interaction between $NPTiO_2$ and $NWTiO_2$ with the acrylate group presented in the organic phase. For this reason, it was possible to prepare hybrid fibers class I with 15 wt % of $NWTiO_2$.

Thermal analysis of hybrid fibers class II showed that both PMMA and PMMA-TiO_2 hybrid material were present in core-shell structures. Moreover, the concentration of the inorganic phase in

percentage by weight was corroborated in hybrid fibers class I. Also, it was demonstrated that a concentration of 5 wt % $NPTiO_2$ increased approximately 10 °C the thermal stability of the material and 12 °C in the case of PMMA—10 wt % $NWTiO_2$. On the other hand, the micromechanical properties showed that at low concentration of $NPTiO_2$ and $NWTiO_2$, Young's modulus magnitude increased in hybrid fibers class I; however, it was PMMA/MMA: TMSPM: TBT 4:1 V/V hybrid fibers that achieved the greatest value of Young's modulus value, thanks to the interaction between the acrylate group and titanium dioxide. Finally, the photocatalytic activity evaluation of the three hybrid materials with various TiO_2 concentrations has shown the photodegradative efficiency of methylene blue, finding that PMMA—10 wt % $NPTiO_2$ hybrid fibers showed greater efficiency, with 94% of methylene blue elimination in an aqueous solution.

Taking into account all of the above, the hybrid fibers class II composed by PMMA/MMA: TMSPM: TBT 4:1 V/V represent the best material for use as an aqueous filtration system, not only because of its good mechanical properties and easy handling, but also for its easy processing by the electrospinning technique and its low cost, where the synthesis of TiO_2 nanoparticles are much less affordable than inorganic precursors for the synthesis of TiO_2 (sol-gel technique). Although PMMA—10 wt % $NPTiO_2$ hybrid fibers reached 94% of methylene blue degradation and PMMA/MMA: TMSPM: TBT 4:1 V/V, they showed only 80% of photodegradation.

ACKNOWLEDGMENTS

The authors thank Silvia Burruel for obtaining the SEM images, Ramon Iñiguez for obtaining the TEM images. F.O.-D. and I.S.-S. also thank CONACYT for the granted scholarship.

REFERENCES

1. Morales-Acosta, M. D.; Quevedo-López, M. A.; Gnade, B. E.; Ramírez-Bon, R. *J. Sol-Gel Sci. Technol.* **2011**, *58*, 218.
2. Almaral-Sánchez, J. L.; Rubio, E.; Mendoza-Galván, A.; Ramírez-Bon, R. *J. Phys. Chem. Solids* **2005**, *66*, 1660.
3. Alvarado-Rivera, J.; Muñoz-Saldaña, J.; Ramírez-Bon, R. *J. Sol-Gel Sci. Technol.* **2010**, *54*, 312.
4. Thavasi, V.; Singh, G.; Ramakrishna, S. *Energy Environ. Sci.* **2008**, *1*, 205.
5. Song, M. Y.; Kim, D. K.; Ihn, K. J.; Jo, S. M.; Kim, D. Y. *Nanotechnology* **2004**, *15*, 1861.
6. Hamadanian, M.; Akbari, A.; Jabbari, V. *Fibers Polym.* **2011**, *12*, 880.
7. Morales-Acosta, M. D.; Alvarado-Beltrán, C. G.; Quevedo-Lopez, M. A.; Gnade, B. E.; Mendoza-Galván, A.; Ramírez-Bon, R. *J. Non-Cryst. Solids* **2013**, *362*, 124.
8. Ramakrishna, S.; Fujihara, K.; Teo, W. -E.; Lim, T. -C.; Ma, Z. An Introduction to Electrospinning and Nanofibers. World Scientific Publishing Co. Pvt. Ltd, Singapore, **2005**.
9. Kim, F. S.; Ren, G.; Jenekhe, S. A. *Chem. Mater.* **2011**, *23*, 682.
10. Li, D.; Xia, Y. *Adv. Mater.* **2004**, *16*, 1151.
11. Dong, Z.; Kennedy, S. J.; Wu, Y. *J. Power Sources* **2011**, *196*, 4886.
12. Pant, H. R.; Bajgai, M. P.; Nam, K. T.; Seo, Y. A.; Pandeya, D. R.; Hong, S. T.; Kim, H. Y. *J. Hazard. Mater.* **2011**, *185*, 124.
13. Im, J. S.; Kim, M. I.; Lee, Y. S. *Mater. Lett.* **2008**, *62*, 3652.
14. Wei, Z.; Li, Y.; Luo, S.; Liu, C.; Meng, D.; Ding, M.; Zeng, G. *Sep. Purif. Technol.* **2014**, *122*, 60.
15. Wang, S. D.; Ma, Q.; Liu, H.; Wang, K.; Zhang, K. Q. *RSC Adv.* **2015**, *5*, 40521.
16. Doh, S. J.; Kim, C.; Lee, S. G.; Lee, S. J.; Kim, H. *J. Hazard. Mater.* **2008**, *154*, 118.
17. Li, H.; Zhang, W.; Li, B.; Pan, W. *J. Am. Ceram. Soc.* **2010**, *93*, 2503.
18. Park, J. Y.; Hwang, K. J.; Lee, J. W.; Lee, I. H. *J. Mater. Sci.* **2011**, *46*, 7240.
19. Li, H.; Zhang, W.; Pan, W. *J. Am. Ceram. Soc.* **2011**, *94*, 3184.
20. Zhou, L.; Wu, N.; Cao, Q.; Jing, B.; Wang, X.; Wang, Q.; Kuang, H. *Solid State Ionics* **2013**, *249*, 93.
21. Piperno, S.; Lozzi, L.; Rastelli, R.; Passacantando, M.; Santucci, S. *Appl. Surf. Sci.* **2006**, *252*, 5583.
22. Macwan, D. P.; Dave, P. N.; Chaturvedi, S. *J. Mater. Sci.* **2011**, *46*, 3669.
23. Alvarado-Beltran, C. G.; Almaral-Sanchez, J. L.; Quevedo-Lopez, M. A.; Ramirez-Bon, R. *Int. J. Electrochem. Sci.* **2015**, 10, 4068.
24. Ngo, V. G.; Bressy, C.; Leroux, C.; Margaillan, A. Synthesis of Hybrid TiO2 Nanoparticles with Well-Defined Poly(methyl Methacrylate) and Poly(Tert-Butyldimethylsilyl Methacrylate) via the RAFT Process. *Polymer (Guildf)* **2009**, *50*, 3095.
25. Du, W.; Wang, H.; Zhong, W.; Shen, L.; Du, Q. High Refractive Index Films Prepared from Titanium Chloride and Methyl Methacrylate via a Non-Aqueous Sol—Gel Route. *J. Sol-Gel Sci. Technol.* **2005**, *34*, 227.
26. Chen, W.; Lee, S.; Lee, L.; Lin, J.; Laboratories, U. C. Synthesis and Characterization of Trialkoxysilane-Capped Poly(methyl methacrylate)-Titania Hybrid Optical Thin Films. **1999**, *9*, 2999.
27. Friederich, B.; Laachachi, A.; Ferriol, M.; Ruch, D.; Cochez, M.; Toniazzo, V. Improvement of Thermal Stability and Fire Behaviour of PMMA by a (Metal Oxide Nanoparticles/Ammonium Polyphosphate/Melamine Polyphosphate) Ternary System. Integrated Systems Design and Technology; Springer, Berlin Heidelberg, pp 47–58, **2010**.